

Observation of Transient Anions That Do Not Decay through Dissociative Electron Attachment: New Pathways for Radiosensitization

Ana I. Lozano,* Fábris Kossoski,* Francisco Blanco, Paulo Limão-Vieira, Márcio T. do N. Varella, and Gustavo García



Cite This: *J. Phys. Chem. Lett.* 2022, 13, 7001–7008



Read Online

ACCESS |



Metrics & More

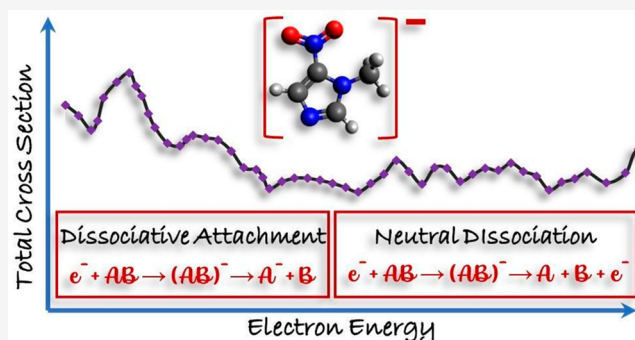


Article Recommendations



Supporting Information

ABSTRACT: Low-energy electrons (LEEs) can very efficiently induce bond breaking via dissociative electron attachment (DEA). While DEA is ubiquitous, the importance of other reactions initiated by LEEs remains much more elusive. Here, we looked into this question by measuring highly accurate total cross sections for electron scattering from 1-methyl-5-nitroimidazole (1MSNI), a model radiosensitizer. The small uncertainty and high energy resolution allow us to identify many resonant features related to the formation of transient anions. In addition to novel insights about DEA reactions through the lower-lying resonances, our key finding is that the higher-lying resonances do not undergo DEA, implying alternative decay channels with significant cross sections. In particular, dissociation into two neutral fragments is probably involved in the case of 1MSNI. This finding has direct implications for the understanding of LEE-induced chemistry, particularly in the fundamental processes underlying the radiosensitization activity.



When a free electron encounters a molecule, the energy from the impinging electron can be efficiently transferred to the molecular target via the formation of a transient anion state.¹ Such states are resonances, meaning they can decay by detachment of the extra electron. When they have long lifetimes against autodetachment, dissociative electron attachment (DEA) becomes likely.² Most molecules are known to undergo DEA, the roles of such processes being numerous and the subject of many studies.^{2–5} Much less is known about the nature and relevance of other chemical processes initiated by electrons, e.g., neutral dissociation. Only recently has bond breaking by the action of a catalytic electron been theoretically proposed^{6,7} and experimentally verified.⁸ This is also a resonant process, taking place via the formation of a transient anion. In this case, however, the electron is released during the reaction, whereas in DEA, it remains attached to one of the fragments. Experimentally, DEA can present sizable cross sections, and the presence of the precursor resonance can be inferred by measurements of the produced ion yields.¹ Alternatively, the resonances can be experimentally probed via accurate measurements of total cross sections (TCSs) for electron scattering,^{9,10} where they usually manifest as prominent features. A remarkable advantage of electron transmission¹¹ (TCS measurements in particular) over DEA experiments is that resonances leave a signature in the cross sections regardless of their decaying mechanisms. As such,

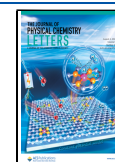
transmission experiments thus allow us to trace other decay processes in addition to DEA, although with no possibility of discerning the process itself.

The role of electron-induced chemistry is increasingly recognized within the context of radiosensitization,^{12–16} although it is a prevalent mechanism in discharges, plasma processing, and nanolithography, among many others.^{17–19} The efficacy of radiotherapy treatments can be significantly improved when deployed in conjunction with radiosensitizer compounds.^{20–22} These molecules act by enhancing the radiosensitivity of tumor tissues and/or cells, thus allowing the delivered doses to be reduced, while minimizing the damage induced by radiotherapy in the neighboring healthy tissues. Although the underlying mechanisms of radiosensitivity remain poorly understood, the production and subsequent chemistry mediated by free radicals certainly play a key role.^{14,15} In particular, low-energy electrons (<10 eV), generated in large numbers along the track of the primary

Received: June 5, 2022

Accepted: July 22, 2022

Published: July 27, 2022



ionization radiation,^{23,24} can efficiently produce free radicals via DEA processes.² This mechanism has motivated the international scientific community to investigate DEA reactions of biologically relevant molecules, with particular relevance to model radiosensitizers.²⁵ In contrast, much less is known about the relevance of other electron-induced processes that do not lead to charged fragments.

Nitroimidazoles (NIs) comprise one of the main classes of candidate radiosensitizers under investigation, in view of their high electron affinities.^{21,26} The most studied NIs are nimorazole, metronidazole, and misonidazole, the first one being currently employed to treat some types of carcinomas in Denmark.²⁷ Their radiosensitizing effect is believed to stem from the action of low-energy electrons, which would produce reactive species when interacting with the NIs.^{28–33} Specifically, DEA reactions have been suggested to be the most relevant underlying process for smaller NIs.^{28–30} More recently, however, the radiosensitivity of nimorazole³¹ and metronidazole³³ has been linked to the formation of the nondecomposed anion via associative electron attachment. Here we put forward a new route for the radiosensitization of NIs, based on the production of neutral fragments via the action of catalytic electrons. It is also worth mentioning that NIs have been proposed as potential candidates for high-energy materials^{34–37} due to their high heats of formation.³⁸ These aspects have motivated several studies on the decomposition of NIs upon collisions with different projectiles.^{28–33,37–43} Of major relevance to the study presented here, Tanzer et al.^{28,29} carried out two experimental investigations of DEA to 4(5)-nitroimidazole [4(5)NI] and its methylated derivatives, 1-methyl-5-nitroimidazole (1MSNI) and 1-methyl-4-nitroimidazole (1M4NI), and obtained the ion yields as a function of the electron impact energy. Several fragment anions were detected between 2 and 6 eV, for the three molecules, despite some differences in their fragmentation pattern. They found that methylation quenches decomposition at the lower impact energies (<2 eV) and, importantly, that no DEA reactions occur above ~6 eV.^{28,29}

In light of the motivations described above, here we looked into the electron–molecule interaction by measuring the first set of total cross sections for 1MSNI, covering a wide energy range (1–300 eV). The choice for 1MSNI was motivated by (i) its structural similarity to the larger nitroimidazolic radiosensitizers nimorazole and metronidazole, (ii) the availability of DEA data,^{28,29} and (iii) the feasibility of measuring the TCS (as discussed below). Energies below 1 eV could not be probed due to a limitation of our experimental setup. Moreover, with the help of multireference configuration interaction (MRCI)⁴⁴ calculations, we provide several novel insights into the nature of the lower-lying resonances and their correspondence to the DEA decay channels. The most important result concerns the observation of several unexpected resonances in the TCS, which have no parallel to the previous experiments on DEA. The obtained TCS is further used to assess the accuracy of two different *ab initio* scattering calculations, the Schwinger multichannel (SMC) method^{45,46} for the lower impact energies (1–15 eV) and the independent atom model with the screening-corrected additivity rule plus interference (IAM-SCAR+I) method^{47–50} for the higher energies (15–300 eV).

The TCS measurements presented here are noteworthy on their own. To the best of our knowledge, few such measurements for gas-phase molecules that are solid at room

temperature have ever been performed, just for fructose,⁵¹ thymine,⁵² phenol,⁵³ and *p*-benzoquinone⁵⁴ (*p*BQ). For the former two molecules, however, only normalized (not absolute) values have been reported, most probably due to the difficulty of assessing the vapor pressure inside the scattering cell.^{10,51,52} Thus, the only sets of absolute TCSs for solid molecular samples have been published a few years ago for phenol⁵³ and *p*BQ,⁵⁴ with our current experimental setup (though in different configurations^{53,54}). Here, we ventured into performing TCS measurements for 1MSNI, a molecule having a vapor pressure at room temperature of $\sim 1.7 \times 10^{-3}$ mmHg,⁵⁵ 2 orders of magnitude lower than those of phenol (0.35 mmHg⁵⁵) and *p*BQ (0.1 mmHg⁵⁵). In addition, we present the most accurate set of TCSs ever obtained with our experimental setup in terms of energy resolution, reaching around 100 meV at lower collision energies. This was paramount for resolving many of the resonant features in the TCS.

In Figure 1, we show our measured TCS, revealing a multitude of resonances formed upon collisions of electrons

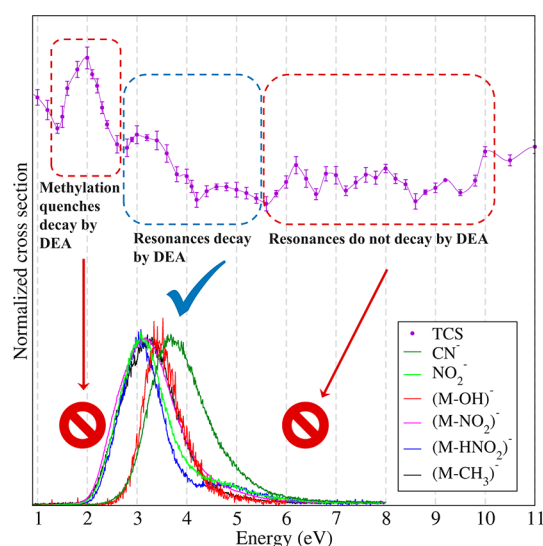


Figure 1. Comparison between our measured TCSs (top) and the ion yields obtained in ref 29 (bottom), with maxima normalized to the same value. The line for the TCS is just a guide for the eye.

with 1MSNI. When compared with the ion yields obtained by Tanzer et al.,²⁹ we notice that only those resonances located between around 2 and 6 eV decay efficiently by DEA. In contrast, we find several overlapping features at higher energies (see Figure 1 and Table S3), related to core-excited resonances. Surprisingly, none of these higher-lying resonances have been observed in DEA experiments.²⁹ Therefore, DEA is largely inefficient for the resonances found in the energy range of 6–10 eV. We thus get to the important conclusion that alternative and efficient decay channels come into play, which may or may not be dissociative. In the former scenario, only neutral fragments should be formed (because there is no signal of DEA).

We argue that neutral dissociation through catalytic electrons^{6,7} (shown schematically in Figure 2 in comparison to DEA) should play a substantial role in the relaxation of these higher-lying resonances. Once the resonance is formed, the electron can be ejected with most of the excess energy, leaving the target molecule in its electronic ground state, but

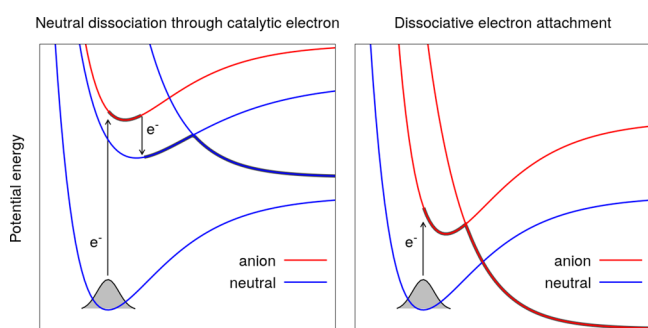


Figure 2. Schematic potential energy curves as a function of a reactive coordinate, illustrating two mechanisms for electron-induced chemistry: neutral dissociation through a catalytic electron (left) and dissociative electron attachment (right).

this would be an unlikely two-particle process. Instead, electron detachment may leave an electronically excited state behind, a more likely one-particle process. There is evidence that the excited states of 1MSNI dissociate into neutral fragments, though not radiatively or via internal conversion to the ground state.³⁷ Yu et al.³⁷ investigated by experimental and theoretical methods the decomposition of NIs, including 1MSNI, upon photoexcitation in the range of 5.0–5.5 eV. They found the NO[•] radical as a product, which would be formed along the potential energy surface of the S₁ excited state, after an internal conversion from the initially excited S₂ state. Our MRCI calculations confirmed the n₋ π₁^{*} (S₁) and n₊ π₁^{*} (S₂) character of these states³⁷ (see the results in the Supporting Information). The same dissociation mechanism would be accessible once the S₂ state is populated after electron collisions. The higher-lying resonances we find in the TCS may decay to higher-lying neutral excited states, followed by a series of internal conversions before reaching the S₂ state and dissociating into the NO[•] radical. On the contrary, entirely different dissociation channels may be accessed from the higher-lying resonances, but again, leading to only uncharged fragments. It is worth mentioning that the NO[•] radical is itself a radiosensitizer.²⁰ From the arguments presented above and the available results for photodissociation of 1MSNI, we believe that dissociation into neutral fragments probably plays an important role in the overall electron-induced chemistry of 1MSNI and NIs in general. Such processes cannot be probed in DEA experiments, which are limited to detecting charged species. The prevalence of such processes remains largely unknown, but our results suggest that they may be more common than previously thought.

The following results and discussion concern the lower energies, where DEA (depicted in Figure 2) is known to occur. The lowest-lying structures (below and around 4 eV) were interpreted in light of MRCI/CCSD(T) calculations (see Computational Methods and Supporting Information for details). Our results for the three lowest-lying valence anion states are in line with the previous work for these states: a bound state (π₁^{*}) and two shape resonances (π₂^{*} and π₃^{*}).⁴¹ The character of the orbitals relevant for the discussion can be seen in Figure S1. From our experimental TCS and calculations, we have further identified and characterized the four lowest-lying core-excited resonances, all of them involving double occupation of the π₁^{*} orbital. Table S3 summarizes every structure found in the TCS, as well as our assignments based on the MRCI/CCSD(T) results.

The most prominent peak in our measured TCSs appears between 1.4 and 2.4 eV, peaking at 2.0 eV. This structure is interpreted as the π₂^{*} shape resonance, theoretically characterized in ref 41. Our measurements thus provide the first experimental confirmation of the π₂^{*} anion state in 1MSNI. No signature of this state has been observed in DEA to 1MSNI, only in its nonmethylated form, implying that methylation quenches DEA reactions below ~2 eV.^{28,29} This comparison highlights the ability of our measurements to identify states that may not manifest in other experimental techniques, as also illustrated in Figure 1. Calculations by Kossoski and Varella⁴¹ suggested that the quenching of DEA reactions below 2 eV would be explained by the very short lifetime against autodetachment of the π₂^{*} resonance in 1MSNI. The favorable comparison between the experimental width [0.71 eV (fitting details are given in the Supporting Information)] and the calculated one (0.53 eV) lends support to this hypothesis. We recall that fixed-nuclei scattering calculations produce overly narrow resonance peaks, such that the purely electronic resonance width from the calculations should be taken as a lower bound to the experiment, making the difference described above more reasonable.

The second most prominent feature in our measured TCS is placed between 2.5 and 4.2 eV. The experimental maximum (3.2 eV) compares very favorably with the calculated ones for the π₃^{*} shape resonance [3.22 eV with the SMC and 3.12 eV with the MRCI/CCSD(T) calculations]. In contrast, the experimental resonance width (1.36 eV) is much larger than the calculated one (0.51 eV). We notice, however, that this peak is considerably more asymmetric than the lower-lying one, with a clear shoulder around 4.0 eV suggesting the presence of other underlying resonances. Indeed, our MRCI/CCSD(T) results support four core-excited resonances between 3.5 and 4.3 eV (see Table S2). From the favorable theoretical–experimental comparisons regarding the π₂^{*} and π₃^{*} shape resonances, we believe that the core-excited resonances would be similarly well described in our calculations, with errors probably below 0.3 eV. We therefore assign the 4.0 eV shoulder to the π₀ (π₁^{*})² core-excited resonance, theoretically predicted at 3.97 eV. Meanwhile, the 3.2 eV peak should stem from the π₃^{*} shape resonance, with some minor contribution from the n₋ (π₁^{*})² core-excited resonance, theoretically found at 3.12 and 3.55 eV, respectively.

Further insights into the underlying DEA reactions are gained once we compare our results with the ion yields reported by Tanzer et al.,²⁹ shown in Figure 1. Above 2 eV, we identify three distinct energy ranges in their measured ion yields. The first one extends from 2 to 6 eV, peaking at around 3 eV, and is common to all fragments involving the nitro group and loss of the methyl group. These DEA channels would be triggered by the π₃^{*} anion state (in this work at ~3.2 eV), which couples to dissociative anion states along the C–NO₂ or N–CH₃ bond.⁴¹ We notice the competition among several dissociation channels for the same resonance. In contrast, production of (1MSNI-OH)⁻ has a distinct profile, narrower in energy and peaking at ~3.4 eV. We assign this fragment to the formation of the n₋ (π₁^{*})² core-excited resonance (found at 3.55 eV in the calculations presented here). In turn, the CN⁻ yield has a maximum at ~3.8 eV and shows a broader energy profile. This DEA channel may be triggered by the π₀ (π₁^{*})² core-excited resonance (identified here at 3.97 eV).

Note that these assignments concern the resonance that probably makes the largest contribution to each dissociation channel. In fact, the fairly broad energy profiles in the ion yields suggest that all of these resonances probably contribute to the same DEA channels. Ribar et al.³⁰ already suggested the existence of a π (π^*)² core-excited resonance at ~ 3.5 eV, based on the prior observations of a shake-up satellite in X-ray photoelectron spectra of NIs⁴⁰ and electron transmission studies on nitroaromatic compounds.⁵⁶ Our results support the presence of such a core-excited resonance and further provide its specific character as π_{O} (π_1^*)². This resonance involves mostly the nitro group, despite some conjugation of the π_1^* orbital with the imidazole group (see Figure S1). As such, it should be common for nitro-containing compounds. In addition to the immediate connection to the studies mentioned above,^{40,56} we further relate the 4 eV shoulder in the TCS (Figure 1) to the peak recently observed in the nitrobenzene TCS measurements at around the same energy.⁵⁷

Extending from 4.2 to 5.6 eV is a broad and somewhat asymmetric feature, with a maximum at ~ 4.7 eV, likely originating from the contribution of several core-excited resonances. Tanzer et al.²⁹ mentioned that structures in the high-energy tail of their measured ion yields could be related to the opening of dissociation channels into more than one neutral species. While this can be an important aspect to consider, the observation of such structures in their ion yields means that additional underlying resonances trigger the dissociation. Indeed, the weak shoulders observed in DEA experiments would be related to some of the higher-lying resonances found in our TCS measurements. The higher-lying roots of our MRCI/CCSD(T) calculations (Table S2) are contained in this region: a π_1 (π_1^*)² core-excited resonance at 4.23 eV and a n_+ (π_1^*)² core-excited resonance at 4.26 eV, though probably more resonances contribute to this broad structure. The only signals in DEA experiments that can be directly correlated with the TCS feature are the formation of NO_2^- and $(1\text{MSNI-HNO}_2)^-$. As discussed above, smaller contributions from higher-lying resonances are expected for most fragments, in view of their generally broad energy profiles. However, it is surprising that resonances displaying a clear increase in the TCS make such a small contribution to DEA (see Figure 1). Except for the somewhat larger signals of $(4(5)\text{NI-HNO}_2)^-$ in this energy range, the ion yields for the nonmethylated compound are quite similar,^{28,29} meaning that a quenching mechanism due to methylation cannot be implied here.

Our TCS further reveals a resonance centered at 6.2 eV, extending from 5.6 to 6.6 eV. It has no obvious correspondence to the ion yield measurements for 1MSNI (or for 1M4NI),²⁹ showing that the underlying resonances do not lead to DEA reactions. In this case, however, 4(5)NI actually undergoes DEA at around the same energies, with distinct features observed for several fragments.²⁹ On the basis of the rather similar energies for the lower-lying resonances,^{29,41} the same would be expected for the resonance(s) at ~ 6 eV. We deduce from the observation of the figures in ref 29 that methylation quenches DEA reactions not only below 2 eV^{28,29} but also around 6 eV. Even then, it is remarkable that the 6.2 eV peak in our TCS is rather intense when compared with the lower-lying structures, whereas in DEA experiments, the signals around 6.2 eV are much weaker than at lower energies. This suggests that these resonances also decay more

efficiently by other mechanisms, as discussed above for the higher-lying resonances.

The measured TCS also served to assess the performance of two *ab initio* electron scattering methodologies, the SMC method for the lower energies and the IAM-SCAR+I method for the intermediate and higher energies, as shown in Figure 3.

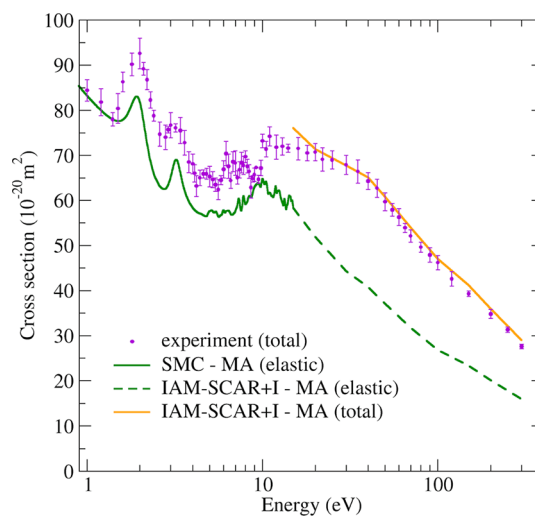


Figure 3. Experimental total electron scattering cross sections from 1MSNI in the energy range of 1–300 eV, together with our IAM-SCAR+I and (elastic) SMC results, considering the experimental angular acceptance (see the text for further details).

To properly compare experimental and theoretical cross sections, special precautions are needed. For each impact energy, we integrated the calculated DCSs over the experimental angular acceptance range, thus ignoring the contribution from forward and backward “missing angles” (MAs) (see Experimental Methods for details). Then, the integrated cross sections were convoluted with a Gaussian having the width of the experimental energy resolution. The final results are depicted in Figure 3 as SMC-MA (elastic) and IAM-SCAR+I-MA (elastic). Adding the inelastic cross sections (ionization and electronic excitation) to the latter further provides a TCS that can be directly compared with the experimental data.

Both magnitudes and the overall shape of TCSs compare quite favorably, which is reassuring for both experimental and theoretical methodologies. The elastic cross sections computed with the SMC method clearly indicate the dominance of the elastic channel at lower energies. The theoretical magnitudes appear to be somewhat underestimated though, which remains to be understood. The positions of the two lowest-lying resonances (around 2.0 and 3.2 eV) are correctly reproduced. The same can be said about the increase in the cross sections at lower energies, related to the long-range interaction mediated by the permanent dipole moment of 1MSNI (4.37 D⁵⁸). Above 4 eV, several weaker features appear in the computed cross sections, which should not be interpreted as physical, given the lack of open electronic excitation channels in our model. The level of agreement between the experiment and the IAM-SCAR+I calculations is excellent at higher energies but no longer holds below ~ 15 eV (not shown), where the IAM-SCAR+I method cannot provide reliable cross sections.^{54,59,60} Even so, it is worth mentioning the good matching at around 15 eV between the SMC and the (elastic)

IAM-SCAR+I results. Finally, the TCS for 1M5NI lies around 10^{-18} m² at the lower energies (~ 1 eV), which is on the same order of magnitude as the associative electron attachment cross sections reported for metronidazole (3.6×10^{-18} m²)³³ and nimorazole (2.8×10^{-18} m²)³¹ close to 0 eV. Despite the different impact energies, systems, and processes, this comparison helps to put the latter cross sections in perspective, highlighting the relevance of associative attachment for metronidazole and nimorazole.

To summarize, here we have employed a state-of-the-art experimental setup for measuring total electron scattering cross sections from 1M5NI, a model molecule for the important class of nitroimidazolic radiosensitizers. The high accuracy and energy resolution reached in this experiment have allowed us to accurately identify many resonances in the TCS, associated with the formation of transient anions. Our main finding is that several of these resonances have no parallel in DEA experiments, showing that alternative decay mechanisms are operative. These higher-lying states are expected to eject slow electrons, thereby populating neutral excited states, which are known to dissociate into neutral fragments based on photodissociation studies by Yu et al.³⁶ We conclude that such neutral dissociation through a catalytic electron mechanism should play a substantial role in the electron-induced decomposition of 1M5NI. Importantly, this mechanism would be accessible for a rather wide energy range [6–10 eV (see Figure 1)], where no DEA takes place. This is an important energy range in the context of radiosensitivity because it coincides with the maximum of the energy distribution of the secondary electrons produced inside biological matter.²³ With only this aspect in mind, processes occurring in the energy range described above (like the neutral dissociation we propose) would be more frequent than those at lower energies (such as DEA), at least in the early stages of thermalization. We notice, however, that the secondary electrons quickly lose their energy to the medium and form much lower energy presolvated states,¹⁵ which could still lead to DEA reactions. Furthermore, neutral dissociation events are expected to be even more chemically relevant than DEA events breaking a single bond, because two radical species (and a released electron) are produced in the former, against only one radical in the latter. While DEA is believed to make a major contribution to the understanding of radiosensitivity,^{12–16} our results point out neutral dissociation through catalytic electrons as a new pathway for radiosensitization. In particular, this pathway represents an alternative radiosensitizing mechanism for nitroimidazolic radiosensitizers, which could play a role similarly important to that of the previously proposed associative attachment (for nimorazole³¹ and metronidazole³³) and DEA (for smaller NIs^{28–30}) electron-induced processes. Detection of neutral fragments remains one of the main experimental challenges in the field of electron–molecule interactions, and we expect our contribution will further encourage the community into looking at this missing puzzle.^{61,62} Our results also shed new light on the transient anions and dissociation pathways of 1M5NI below 4 eV and on the effect of methylation in suppressing DEA reactions between 4 and 6 eV. Finally, the study presented here demonstrates that accurate measurements of absolute TCS for solid compounds having a room-temperature vapor pressure as low as $\sim 10^{-3}$ mmHg are technically feasible. This opens the possibility of performing analogous studies for electron

interactions with molecules having comparable low vapor pressures.

EXPERIMENTAL METHODS

The TCS measurements were carried out in a state-of-the-art magnetically confined electron beam system described in detail elsewhere.^{60,63} Further details about the experimental methods can be found in section S1 of the Supporting Information. Considering that 1M5NI is solid and has a very low vapor pressure at room temperature ($\sim 1.7 \times 10^{-3}$ mmHg⁵⁵), obtaining the measurements presented here has represented a major experimental challenge. The main reason is that absolute values of TCS require accurate and stable measurements of the sample's gas pressure inside the collision chamber, which becomes increasingly difficult for lower-vapor pressure compounds. The sample was heated to around 333 K. At the same time, the temperature was controlled to maintain it in a range where thermal dissociation does not occur. In addition, the collision chamber's temperature was kept around 20–30 K above the sample's temperature, thus preventing condensation effects.

Although the total statistical uncertainties of these measurements remain below 5%, our measured TCSs lay lower than the “real” values due to the experimental angular acceptance. Concretely, in the experimental system presented here, the angular resolution is linked to the energy resolution as a consequence of the magnetic confinement, entailing thus “missing angles” in the forward and backward scattering directions, as explained in detail in ref 63. Therefore, this should be considered when the results derived from this setup are compared with other, experimental^{60,64} but also theoretical results. The experimental TCSs presented here together with their absolute uncertainties are listed in Table S1.

COMPUTATIONAL METHODS

To quantitatively characterize the lower-lying shape and core-excited resonances of 1M5NI, we resorted to bound-state MRCI calculations. By building proper state-average reference wave functions, we aim at a more balanced description of both (one-particle) shape and (two-particle) core-excited resonances. Being a bound-state method, couplings to the continuum are neglected. However, we verified that all of the obtained roots correspond to localized states (and not some discretization of the continuum), thus reassuring us that our MRCI calculations would provide a decent description of the resonances. The relative energies among neutral states and among anion states are expected to be reasonable with our MRCI calculations. That would not be the case, however, when comparing neutral and anion energies, because the latter appear to be too high with respect to the former. This is due to the well-known challenges associated with a balanced description of correlation effects in neutral and charged forms. To correct for that, we have performed separate calculations for the neutral and anion ground states, at the coupled cluster with singles, doubles, and perturbative triples [CCSD(T)] levels.^{65,66} Then, we introduced a systematic shift into all energies of the anion states, based on the CCSD(T) binding energy. More precisely, the herein reported resonance energy for the *i*th anion state, E_r^i , was obtained from the equation $E_r^i = E_{\text{CCSD(T)}}^1 - E_{\text{CCSD(T)}}^N + E_{\text{MRCI}}^i - E_{\text{MRCI}}^1$, where $E_{\text{CCSD(T)}}^1$ and $E_{\text{CCSD(T)}}^N$ are the CCSD(T) energies of the anion ground state ($i = 1$) and the neutral ground state,

respectively, and E_{MRCI}^i and E_{MRCI}^1 are the MRCI energies (plus Pople's extensivity correction⁶⁷) of the i th anion state and the anion ground state ($i = 1$), respectively. Throughout the text, we refer to this mixed set of calculations as MRCI/CCSD(T). Due to the high computational cost of these calculations, a limited number of states were obtained (seven for each charge state), thus restricting our theoretical analysis to energies below ~ 4 eV.

Further methodological details concerning the bound-state MRCI and electron scattering IAM-SCAR+I and SMC calculations are given in section S2 of the Supporting Information. We notice that the current implementation of the SMC method usually provides one-particle shape resonance energies within ~ 0.3 eV of the experimental values, though it still struggles to describe two-particle core-excited resonances.^{68,69} For this reason, we resorted to bound-state MRCI calculations to describe these states.

■ ASSOCIATED CONTENT

SI Supporting Information

The Supporting Information is available free of charge at <https://pubs.acs.org/doi/10.1021/acs.jpcllett.2c01704>.

Experimental and theoretical details, measured total electron scattering cross sections and their absolute uncertainties, active orbitals in the CASSCF calculations, vertical excitation energies, resonance energies of the anion states, and a Gaussian fit of the two lowest-lying peaks (PDF)

Transparent Peer Review report available (PDF)

■ AUTHOR INFORMATION

Corresponding Authors

Fábris Kossoski – *Laboratoire de Chimie et Physique Quantiques (UMR 5626), Université de Toulouse, CNRS, UPS, 31062 Toulouse, France*; orcid.org/0000-0002-1627-7093; Email: fkossoski@irsamc.ups-tlse.fr

Ana I. Lozano – *Instituto de Física Fundamental, Consejo Superior de Investigaciones Científicas, 28006 Madrid, Spain; Laboratório de Colisões Atômicas e Moleculares, CEFITEC, Departamento de Física, Faculdade de Ciências e Tecnologia, Universidade NOVA de Lisboa, 2829-516 Caparica, Portugal*; orcid.org/0000-0003-4613-0372; Email: ai.lozano@fct.unl.pt

Authors

Franco Blanco – *Departamento de Física Atómica, Molecular y Nuclear, Universidad Complutense de Madrid, 28040 Madrid, Spain*

Paulo Limão-Vieira – *Laboratório de Colisões Atômicas e Moleculares, CEFITEC, Departamento de Física, Faculdade de Ciências e Tecnologia, Universidade NOVA de Lisboa, 2829-516 Caparica, Portugal*; orcid.org/0000-0003-2696-1152

Márcio T. do N. Varela – *Instituto de Física, Universidade de São Paulo, 05508-090 São Paulo, Brazil*; orcid.org/0000-0002-5812-0342

Gustavo García – *Instituto de Física Fundamental, Consejo Superior de Investigaciones Científicas, 28006 Madrid, Spain; Centre for Medical Radiation Physics, University of Wollongong, Wollongong 2522 NSW, Australia*

Complete contact information is available at:

<https://pubs.acs.org/doi/10.1021/acs.jpcllett.2c01704>

Notes

The authors declare no competing financial interest.

■ ACKNOWLEDGMENTS

This study has been partially supported by the Spanish Ministerio de Ciencia e Innovación (Project PID2019-104727RB-C21), Ministerio de Universidades (Project PRX21/00340), and CSIC (Project LINKA20085). A.I.L. and P.L.-V. acknowledge the Portuguese National Funding Agency (FCT) through research Grants CEFITEC (UIDB/00068/2020) and PTDC/FIS-AQM/31281/2017. M.T.d.N.V. acknowledges the Brazilian National Council for Scientific and Technological Development (CNPq, Grant 304571/2018-0) and the São Paulo Research Foundation (FAPESP, Grant 2020/16155-7). The authors also thank Prof. Stephan Denifl from the University of Innsbruck for providing published data on DEA to IMSNI.

■ REFERENCES

- (1) Schulz, G. J. Resonances in Electron Impact on Diatomic Molecules. *Rev. Mod. Phys.* **1973**, *45* (3), 423–486.
- (2) Fabrikant, I. I.; Eden, S.; Mason, N. J.; Fedor, J. Recent Progress in Dissociative Electron Attachment. *Advances in Atomic, Molecular, and Optical Physics* **2017**, *66*, 545–657.
- (3) Ingolfsson, O. *Low-Energy Electrons: Fundamentals and Applications*; Jenny Stanford Publishing: Boca Raton, FL, 2019.
- (4) Pshenichnyuk, S. A.; Modelli, A.; Komolov, A. S. Interconnections between Dissociative Electron Attachment and Electron-Driven Biological Processes. *Int. Rev. Phys. Chem.* **2018**, *37* (1), 125–170.
- (5) Pshenichnyuk, S. A.; Asfandiarov, N. L.; Vorob'ev, A. S.; Matejčík, Š. State of the Art in Dissociative Electron Attachment Spectroscopy and Its Prospects. *Physics-Uspokhi* **2022**, *65* (2), 163–188.
- (6) Davis, D.; Vysotskiy, V. P.; Sajeev, Y.; Cederbaum, L. S. Electron Impact Catalytic Dissociation: Two-Bond Breaking by a Low-Energy Catalytic Electron. *Angew. Chemie Int. Ed.* **2011**, *50* (18), 4119–4122.
- (7) Davis, D.; Vysotskiy, V. P.; Sajeev, Y.; Cederbaum, L. S. A One-Step Four-Bond-Breaking Reaction Catalyzed by an Electron. *Angew. Chemie Int. Ed.* **2012**, *51* (32), 8003–8007.
- (8) Davis, D.; Kundu, S.; Prabhudesai, V. S.; Sajeev, Y.; Krishnakumar, E. Formation of CO₂ from Formic Acid through Catalytic Electron Channel. *J. Chem. Phys.* **2018**, *149* (6), 064308.
- (9) Brunger, M. J. Molecular Processes and Techniques for Measuring Their Scattering Cross Sections. In *Low-Energy Electrons*; Jenny Stanford Publishing: Boca Raton, FL, 2019; pp 1–46.
- (10) Szymkowski, C.; Mozejko, P. Recent Total Cross Section Measurements in Electron Scattering from Molecules. *Eur. Phys. J. D* **2020**, *74* (5), 90.
- (11) Jordan, K. D.; Burrow, P. D. Temporary Anion States of Polyatomic Hydrocarbons. *Chem. Rev.* **1987**, *87* (3), 557–588.
- (12) Alizadeh, E.; Orlando, T. M.; Sanche, L. Biomolecular Damage Induced by Ionizing Radiation: The Direct and Indirect Effects of Low-Energy Electrons on DNA. *Annu. Rev. Phys. Chem.* **2015**, *66* (1), 379–398.
- (13) Schürmann, R.; Tsering, T.; Tanzer, K.; Denifl, S.; Kumar, S. V. K.; Bald, I. Resonant Formation of Strand Breaks in Sensitized Oligonucleotides Induced by Low-Energy Electrons (0.5–9 eV). *Angew. Chemie Int. Ed.* **2017**, *56* (36), 10952–10955.
- (14) Schürmann, R.; Vogel, S.; Ebel, K.; Bald, I. The Physico-Chemical Basis of DNA Radiosensitization: Implications for Cancer Radiation Therapy. *Chem. - A Eur. J.* **2018**, *24* (41), 10271–10279.
- (15) Kumar, A.; Becker, D.; Adhikary, A.; Sevilla, M. D. Reaction of Electrons with DNA: Radiation Damage to Radiosensitization. *Int. J. Mol. Sci.* **2019**, *20* (16), 3998.
- (16) Ebel, K.; Bald, I. Low-Energy (5–20 eV) Electron-Induced Single and Double Strand Breaks in Well-Defined DNA Sequences. *J. Phys. Chem. Lett.* **2022**, *13*, 4871–4876.

- (17) Arumainayagam, C. R.; Lee, H.-L.; Nelson, R. B.; Haines, D. R.; Gunawardane, R. P. Low-Energy Electron-Induced Reactions in Condensed Matter. *Surf. Sci. Rep.* **2010**, *65* (1), 1–44.
- (18) Böhrer, E.; Warneke, J.; Swiderek, P. Control of Chemical Reactions and Synthesis by Low-Energy Electrons. *Chem. Soc. Rev.* **2013**, *42* (24), 9219–9231.
- (19) Arumainayagam, C. R.; Garrod, R. T.; Boyer, M. C.; Hay, A. K.; Bao, S. T.; Campbell, J. S.; Wang, J.; Nowak, C. M.; Arumainayagam, M. R.; Hodge, P. J. Extraterrestrial Prebiotic Molecules: Photochemistry vs. Radiation Chemistry of Interstellar Ices. *Chem. Soc. Rev.* **2019**, *48* (8), 2293–2314.
- (20) Wardman, P. Chemical Radiosensitizers for Use in Radiotherapy. *Clin. Oncol.* **2007**, *19* (6), 397–417.
- (21) Gong, L.; Zhang, Y.; Liu, C.; Zhang, M.; Han, S. Application of Radiosensitizers in Cancer Radiotherapy. *Int. J. Nanomedicine* **2021**, *16*, 1083–1102.
- (22) Zdrowowicz, M.; Chomicz-Mańka, L.; Butowska, K.; Spisz, P.; Falkiewicz, K.; Czaja, A.; Rak, J. DNA Damage Radiosensitizers Geared Towards Hydrated Electrons. In *Practical Aspects of Computational Chemistry V*; Springer International Publishing: Cham, Switzerland, 2022; pp 125–169.
- (23) Pimblott, S. M.; LaVerne, J. A. Production of Low-Energy Electrons by Ionizing Radiation. *Radiat. Phys. Chem.* **2007**, *76* (8–9), 1244–1247.
- (24) Alizadeh, E.; Sanche, L. Precursors of Solvated Electrons in Radiobiological Physics and Chemistry. *Chem. Rev.* **2012**, *112* (11), 5578–5602.
- (25) Gorfinkiel, J. D.; Ptasińska, S. Electron Scattering from Molecules and Molecular Aggregates of Biological Relevance. *J. Phys. B At. Mol. Opt. Phys.* **2017**, *50* (18), 182001.
- (26) Wang, H.; Mu, X.; He, H.; Zhang, X.-D. Cancer Radiosensitizers. *Trends Pharmacol. Sci.* **2018**, *39* (1), 24–48.
- (27) Henk, J. M.; Bishop, K.; Shepherd, S. F. Treatment of Head and Neck Cancer with CHART and Nimorazole: Phase II Study. *Radiother. Oncol.* **2003**, *66* (1), 65–70.
- (28) Tanzer, K.; Feketeová, L.; Puschnigg, B.; Scheier, P.; Illenberger, E.; Denifl, S. Reactions in Nitroimidazole Triggered by Low-Energy (0–2 eV) Electrons: Methylation at N1-H Completely Blocks Reactivity. *Angew. Chemie - Int. Ed.* **2014**, *53* (45), 12240–12243.
- (29) Tanzer, K.; Feketeová, L.; Puschnigg, B.; Scheier, P.; Illenberger, E.; Denifl, S. Reactions in Nitroimidazole and Methylnitroimidazole Triggered by Low-Energy (0–8 eV) Electrons. *J. Phys. Chem. A* **2015**, *119* (25), 6668–6675.
- (30) Ribar, A.; Fink, K.; Probst, M.; Huber, S. E.; Feketeová, L.; Denifl, S. Isomer Selectivity in Low-Energy Electron Attachment to Nitroimidazoles. *Chem. - A Eur. J.* **2017**, *23* (52), 12892–12899.
- (31) Meißner, R.; Kočíšek, J.; Feketeová, L.; Fedor, J.; Fárnik, M.; Limão-Vieira, P.; Illenberger, E.; Denifl, S. Low-Energy Electrons Transform the Nimorazole Molecule into a Radiosensitizer. *Nat. Commun.* **2019**, *10* (1), 2388.
- (32) Meißner, R.; Feketeová, L.; Illenberger, E.; Denifl, S. Reactions in the Radiosensitizer Misonidazole Induced by Low-Energy (0–10 eV) Electrons. *Int. J. Mol. Sci.* **2019**, *20* (14), 3496.
- (33) Lochmann, C.; Luxford, T. F. M.; Makurat, S.; Pysanenko, A.; Kočíšek, J.; Rak, J.; Denifl, S. Low-Energy Electron Induced Reactions in Metronidazole at Different Solvation Conditions. *Pharmaceuticals* **2022**, *15* (6), 701.
- (34) Cho, J. R.; Kim, K. J.; Cho, S. G.; Kim, J. K. Synthesis and Characterization of 1-Methyl-2,4,5-Trinitroimidazole (MTNI). *J. Heterocycl. Chem.* **2002**, *39* (1), 141–147.
- (35) Nair, U.; Asthana, S.; Rao, A.; Gandhe, B. Advances in High Energy Materials. *Def. Sci. J.* **2010**, *60* (2), 137–151.
- (36) Yu, Z.; Bernstein, E. R. Experimental and Theoretical Studies of the Decomposition of New Imidazole Based Energetic Materials: Model Systems. *J. Chem. Phys.* **2012**, *137* (11), 114303.
- (37) Yu, Z.; Bernstein, E. R. On the Decomposition Mechanisms of New Imidazole-Based Energetic Materials. *J. Phys. Chem. A* **2013**, *117* (8), 1756–1764.
- (38) Carvalho, T. M. T.; Amaral, L. M. P. F.; Morais, V. M. F.; Ribeiro da Silva, M. D. M. C. Calorimetric and Computational Studies for Three Nitroimidazole Isomers. *J. Chem. Thermodyn.* **2017**, *105*, 267–275.
- (39) Feketeová, L.; Plekan, O.; Goonewardane, M.; Ahmed, M.; Albright, A. L.; White, J.; O'Hair, R. A. J.; Horsman, M. R.; Wang, F.; Prince, K. C. Photoelectron Spectra and Electronic Structures of the Radiosensitizer Nimorazole and Related Compounds. *J. Phys. Chem. A* **2015**, *119* (39), 9986–9995.
- (40) Itälä, E.; Tanzer, K.; Granroth, S.; Kooser, K.; Denifl, S.; Kukuk, E. Fragmentation Patterns of 4(5)-Nitroimidazole and 1-Methyl-5-Nitroimidazole — The Effect of the Methylation. *J. Mass Spectrom.* **2017**, *52* (11), 770–776.
- (41) Kossoski, F.; Varella, M. T. do N. How Does Methylation Suppress the Electron-Induced Decomposition of 1-Methyl-Nitroimidazoles? *J. Chem. Phys.* **2017**, *147* (16), 164310.
- (42) Mendes, M.; Probst, M.; Maihom, T.; García, G.; Limão-Vieira, P. Selective Bond Excision in Nitroimidazoles by Electron Transfer Experiments. *J. Phys. Chem. A* **2019**, *123* (18), 4068–4073.
- (43) Mendes, M.; García, G.; Bacchus-Montabonel, M. C.; Limão-Vieira, P. Electron Transfer Induced Decomposition in Potassium–Nitroimidazoles Collisions: An Experimental and Theoretical Work. *Int. J. Mol. Sci.* **2019**, *20* (24), 6170.
- (44) Szalay, P. G.; Müller, T.; Gidofalvi, G.; Lischka, H.; Shepard, R. Multiconfiguration Self-Consistent Field and Multireference Configuration Interaction Methods and Applications. *Chem. Rev.* **2012**, *112* (1), 108–181.
- (45) Takatsuka, K.; McKoy, V. Extension of the Schwinger Variational Principle beyond the Static-Exchange Approximation. *Phys. Rev. A* **1981**, *24* (5), 2473–2480.
- (46) da Costa, R. F.; Varella, M. T. do N.; Betttega, M. H. F.; Lima, M. A. P. Recent Advances in the Application of the Schwinger Multichannel Method with Pseudopotentials to Electron-Molecule Collisions. *Eur. Phys. J. D* **2015**, *69* (6), 159.
- (47) Blanco, F.; García, G. Screening Corrections for Calculation of Electron Scattering Differential Cross Sections from Polyatomic Molecules. *Phys. Lett. A* **2004**, *330* (3–4), 230–237.
- (48) Blanco, F.; Rosado, J.; Illana, A.; García, G. Comparison of Two Screening Corrections to the Additivity Rule for the Calculation of Electron Scattering from Polyatomic Molecules. *Phys. Lett. A* **2010**, *374* (43), 4420–4424.
- (49) Blanco, F.; Ellis-Gibbings, L.; García, G. Screening Corrections for the Interference Contributions to the Electron and Positron Scattering Cross Sections from Polyatomic Molecules. *Chem. Phys. Lett.* **2016**, *645*, 71–75.
- (50) Dubuis, A. T.; Costa, F.; da Silva, F. F.; Limão-Vieira, P.; Oller, J. C.; Blanco, F.; García, G. Total Electron Scattering Cross Section from Pyridine Molecules in the Energy Range 10–1000 eV. *Chem. Phys. Lett.* **2018**, *699*, 182–187.
- (51) Chernyshova, I. V.; Kontrosh, E. E.; Markush, P. P.; Shpenik, O. B. The Interaction of Low-Energy Electrons with Fructose Molecules. *Technol. Phys. Lett.* **2017**, *43* (11), 998–1000.
- (52) Chernyshova, I. V.; Kontrosh, E. E.; Shpenik, O. B. Collisions of Slow Electrons with Thymine Molecules. *Opt. Spectrosc.* **2018**, *125* (6), 845–852.
- (53) da Costa, R. F.; de Oliveira, E. M.; Betttega, M. H. F.; Varella, M. T. do N.; Jones, D. B.; Brunger, M. J.; Blanco, F.; Colmenares, R.; Limão-Vieira, P.; García, G.; Lima, M. A. P. Electron Collisions with Phenol: Total, Integral, Differential, and Momentum Transfer Cross Sections and the Role of Multichannel Coupling Effects on the Elastic Channel. *J. Chem. Phys.* **2015**, *142* (10), 104304.
- (54) Lozano, A. I.; Oller, J. C.; Jones, D. B.; da Costa, R. F.; Varella, M. T. do N.; Betttega, M. H. F.; Ferreira da Silva, F.; Limão-Vieira, P.; Lima, M. A. P.; White, R. D.; Brunger, M. J.; Blanco, F.; Muñoz, A.; García, G. Total Electron Scattering Cross Sections from Parabenzoquinone in the Energy Range 1–200 eV. *Phys. Chem. Chem. Phys.* **2018**, *20* (34), 22368–22378.
- (55) U.S. National Library of Medicine. <https://chem.nlm.nih.gov> (accessed 2022-06-01).

(56) Modellia, A.; Venuti, M. Empty Level Structure and Dissociative Electron Attachment in Gas-Phase Nitro Derivatives. *Int. J. Mass Spectrom.* **2001**, *205* (1–3), 7–16.

(57) Álvarez, L.; Costa, F.; Lozano, A. I.; Oller, J. C.; Muñoz, A.; Blanco, F.; Limão-Vieira, P.; White, R. D.; Brunger, M. J.; García, G. Electron Scattering Cross Sections from Nitrobenzene in the Energy Range 0.4–1000 eV: The Role of Dipole Interactions in Measurements and Calculations. *Phys. Chem. Chem. Phys.* **2020**, *22* (24), 13505–13515.

(58) Pandeti, S.; Feketeová, L.; Reddy, T. J.; Abdoul-Carime, H.; Farizon, B.; Farizon, M.; Märk, T. D. Nitroimidazolic Radiosensitizers Investigated by Electrospray Ionization Time-of-Flight Mass Spectrometry and Density Functional Theory. *RSC Adv.* **2017**, *7* (71), 45211–45221.

(59) Lozano, A. I.; Loupas, A.; Blanco, F.; Gorfinkiel, J. D.; García, G. Total Electron Scattering Cross Sections from Thiophene for the (1–300 eV) Impact Energy Range. *J. Chem. Phys.* **2018**, *149* (13), 134303.

(60) García-Abenza, A.; Lozano, A. I.; Álvarez, L.; Oller, J. C.; Blanco, F.; Stokes, P.; White, R. D.; Urquijo, J. d.; Limão-Vieira, P.; Jones, D. B.; Brunger, M. J.; García, G. A Complete Data Set for the Simulation of Electron Transport through Gaseous Tetrahydrofuran in the Energy Range 1–100 eV. *Eur. Phys. J. D* **2021**, *75* (12), 303.

(61) Li, Z.; Milosavljević, A. R.; Carmichael, I.; Ptasinska, S. Characterization of Neutral Radicals from a Dissociative Electron Attachment Process. *Phys. Rev. Lett.* **2017**, *119* (5), 053402.

(62) Ptasinska, S. A Missing Puzzle in Dissociative Electron Attachment to Biomolecules: The Detection of Radicals. *Atoms* **2021**, *9* (4), 77.

(63) Lozano, A. I.; Oller, J. C.; Krupa, K.; Ferreira da Silva, F.; Limão-Vieira, P.; Blanco, F.; Muñoz, A.; Colmenares, R.; García, G. Magnetically Confined Electron Beam System for High Resolution Electron Transmission-Beam Experiments. *Rev. Sci. Instrum.* **2018**, *89* (6), 063105.

(64) Costa, F.; Traoré-Dubuis, A.; Álvarez, L.; Lozano, A. I.; Ren, X.; Dorn, A.; Limão-Vieira, P.; Blanco, F.; Oller, J. C.; Muñoz, A.; García-Abenza, A.; Gorfinkiel, J. D.; Barbosa, A. S.; Bettega, M. H. F.; Stokes, P.; White, R. D.; Jones, D. B.; Brunger, M. J.; García, G. A Complete Cross Section Data Set for Electron Scattering by Pyridine: Modelling Electron Transport in the Energy Range 0–100 eV. *Int. J. Mol. Sci.* **2020**, *21* (18), 6947.

(65) Purvis, G. D.; Bartlett, R. J. A Full Coupled-cluster Singles and Doubles Model: The Inclusion of Disconnected Triples. *J. Chem. Phys.* **1982**, *76* (4), 1910–1918.

(66) Raghavachari, K.; Trucks, G. W.; Pople, J. A.; Head-Gordon, M. A Fifth-Order Perturbation Comparison of Electron Correlation Theories. *Chem. Phys. Lett.* **1989**, *157* (6), 479–483.

(67) Pople, J. A.; Seeger, R.; Krishnan, R. Variational Configuration Interaction Methods and Comparison with Perturbation Theory. *Int. J. Quantum Chem.* **1977**, *12* (S11), 149–163.

(68) da Costa, R. F.; Ruivo, J. C.; Kossoski, F.; Varella, M. T. do N.; Bettega, M. H. F.; Jones, D. B.; Brunger, M. J.; Lima, M. A. P. An Ab Initio Investigation for Elastic and Electronically Inelastic Electron Scattering from Para-Benzoquinone. *J. Chem. Phys.* **2018**, *149* (17), 174308.

(69) Moreira, G. M.; Kossoski, F.; Bettega, M. H. F.; Costa, R. F. da. Electronic Excitation of the 3B_2 State of Thiophene Molecule by Low-Energy Electron Collisions. *J. Phys. B At. Mol. Opt. Phys.* **2020**, *53* (8), 08S002.

Recommended by ACS

Ejecting Electrons from Molecular Anions via Shine, Shake/Rattle, and Roll

Jack Simons.

SEPTEMBER 26, 2020
THE JOURNAL OF PHYSICAL CHEMISTRY A

READ 

Role of Nonvalence States in the Ultrafast Dynamics of Isolated Anions

Jan R. R. Verlet, Joshua P. Rogers, *et al.*

APRIL 01, 2020
THE JOURNAL OF PHYSICAL CHEMISTRY A

READ 

Multi-Basis-Set (TD-)DFT Methods for Predicting Electron Attachment Energies

Guillaume Thiam and Franck Rabilloud

OCTOBER 07, 2021
THE JOURNAL OF PHYSICAL CHEMISTRY LETTERS

READ 

Localized and Delocalized States of a Diamine Cation: Resolution of a Controversy

Marta Gałyńska, Ragnar Björnsson, *et al.*

JANUARY 26, 2021
THE JOURNAL OF PHYSICAL CHEMISTRY LETTERS

READ 

Get More Suggestions >